Robustness of Vegetation Optical Depth Retrievals Based on L-Band Global Radiometry

David Chaparro, Andrew F. Feldman, *Member, IEEE*, Mario Julian Chaubell,
Simon H. Yueh, *Fellow, IEEE*, and Dara Entekhabi, *Fellow, IEEE*

Abstract—Microwave vegetation optical depth (VOD) and soil moisture (SM) can be simultaneously retrieved based on L-band radiometry with polarization information. VOD is indicative of the vegetation water content (VWC) because it captures the extinction of land surface emission. If the connectivity of VOD to VWC is robust, the pair of VWC-SM observations can be viable bases for understanding soil–plant–atmosphere water relations, providing new perspectives on ecosystem science. Simultaneous SM–VOD retrievals are feasible by inverting the $\tau - \omega$ model with two independent datasets in dual-channel algorithms. However, given correlated satellite vertical and horizontal brightness temperatures (TBs; TB_v and TB_h), an ill-posed inverse problem arises where TB errors result in high uncertainties of retrievals. In this study, we apply the degrees-of-information (DoI) metric and propose a signal-to-noise ratio (SNR) metric to assess the "retrievability" of VOD given the Soil Moisture Active Passive (SMAP) TB_v–TB_h linear dependence. The application of these metrics allows determining where the VOD retrievals are robust and reliable. This is a necessary step in supporting the applications of VOD in ecology and hydrology. Results show that regions with mainly nonwoody vegetation have the best potential for VOD retrievals, though regularization is necessary. We then assess VOD time variations from two regularization products that reduce the impact of underdetermined inversions: the L3 dual-channel algorithm (L3-DCA) and the multitemporal dual-channel algorithm (MTDCA), which constrain VOD time dynamics with and without using *a priori* VOD climatology, respectively. Though they both reduce noise, especially in the VOD retrievals, they result in differences in VOD seasonal amplitude and coupling to SM at high frequencies as we outline here.

Index Terms—Microwave retrieval algorithms, regularization, soil moisture (SM), Soil Moisture Active Passive (SMAP), vegetation optical depth (VOD) robustness.

David Chaparro is with the Microwaves and Radar Institute, German Aerospace Center, 82234 Weßling, Germany, and also with CommSensLab, Universitat Politècnica de Catalunya (UPC)/IEEC, 08034 Barcelona, Spain (e-mail: david.chaparrodanon@dlr.de).

Andrew F. Feldman is with the NASA Postdoctoral Program, Biospheric Sciences Laboratory, NASA Goddard Space Flight Center, Greenbelt, MD 20771 USA (e-mail: afeld24@mit.edu).

Mario Julian Chaubell and Simon H. Yueh are with the Jet Propulsion Laboratory, California Institute of Technology, Pasadena, CA 91109 USA (e-mail: mario.j.chaubell@jpl.nasa.gov; simon.h.yueh@jpl.nasa.gov).

Dara Entekhabi is with the Department of Civil and Environmental Engineering, Massachusetts Institute of Technology, Cambridge, MA 02139 USA (e-mail: darae@mit.edu).

I. INTRODUCTION

MICROWAVE radiometers on board the Soil Moisture Active Passive (SMAP; launched in 2015 [1]) and Soil Moisture and Ocean Salinity (SMOS; launched in 2009 [2]) satellites measure the Earth's microwave surface emission at a low frequency (L-band, 1.4 GHz). Over land, such measurements are sensitive to the rough surface reflectivity and to the attenuation and scattering that the entire vegetation canopy exerts over the surface emission. The rough surface reflectivity is related to the soil dielectric constant and electromagnetic roughness. The inversion of estimated surface reflectivity results in estimates of surface soil moisture (SM). A by-product of the retrieval is the amount of vegetation attenuation and scattering that together are captured by the vegetation optical depth (VOD). VOD is known to be related to the vegetation water content (VWC), the vegetation biomass, and the plants' structure [3], [4], [5].

SM and VOD are valuable hydrologic and ecological indicators important for a breadth of applications and studies. These include biomass estimation (e.g., [6], [7], [8]), crop yield assessment [9], [10], development of drought indicators (e.g., [11]), study of drought-derived tree mortality [12], estimation of vegetation moisture [13], [14], and analyses of water exchange in the soil–plant–atmosphere continuum [15], [16], [17].

The estimates of global SM fields based on SMAP and SMOS L-band measurements are routinely assessed against widely available *in situ* SM probe measurements. In contrast, there are only few studies reporting how well VOD represents *in situ* plant physiology and phenology (e.g., [18]). Studies of how well VOD represents VWC at the satellite scale are becoming more prevalent [4], [5], [15], [19], [20], [21]. These assessments are based on sparse tower measurements and crop models, which are highly informative. However, VOD

in situ measurements are sparse, leaving only limited or indirect methods for global assessment. Thus, there is still a need to determine where and to what degree VOD is more robust to satellite measurement error. The concern arises from the retrieval of two parameters (VOD and SM) from two measurements [polarized brightness temperatures (TBs)] that are correlated [22].

To retrieve simultaneously SM and VOD, the inversion of a zeroth-order radiative transfer model (the $\tau - \omega$ model [23]) is commonly applied. This requires at least two independent sources of information in order to minimize the cost function that links measured and estimated TBs to retrieve the appropriate SM–VOD pairs. Different approaches are considered depending on each sensor and algorithm. For the SMOS satellite, its multiangular and dual-polarization configuration allows obtaining SM and VOD simultaneously without the need of ancillary information [24]. For SMAP, with one incidence angle ($\theta = 40°$), VOD is derived from ancillary information in order to retrieve SM when only one polarization is used (i.e., the single-channel algorithm (SCA) [25]). Alternatively, both horizontal and vertical polarizations are applied in the dual-channel algorithm (DCA) to simultaneously retrieve SM and VOD [26]. Nevertheless, these TBs at horizontal (TB_h) and vertical (TB_v) polarizations are often correlated, containing redundant information [27]. Thus, they are not independent measurements, and their differences can be dominated by instrument error. As a result, DCA approaches are ill-posed and can lead to difficulty in algorithmic gradient search methods finding the true SM and VOD values for a given snapshot [28].

Therefore, the underdetermination of the VOD and SM inversion due to correlated polarization measurements is expected to introduce noise into the retrievals. We expect that the noise has different characteristics at different frequencies. At longer time scales such as the seasonal cycle, we expect that the various approaches to regularize the inversion yield similar results. Indeed, Zwieback *et al.* [29], Feldman *et al.* [30], and Gao *et al.* [31] showed that the seasonal cycles of the various approaches are similar and the climatologies of VOD are comparable. Our concern, however, is that the noise at much higher frequencies such as the overpass-to-overpass or the Nyquist frequency may be at different levels depending on the approach to the inversion. This would impact studies that examine short-time scale (i.e., subweekly to monthly) covariations in VOD and SM, such as the study of the soil–plant–atmosphere water dynamics. Most other studies that examine climatologies of VOD (e.g., those focusing on aboveground biomass, crop phenology, and so on) may be less affected.

In order to quantify how well-posed the inversion is, previous work estimates the degrees-of-information (DoI) metric (DoI is defined in [22] and measures the fractional amount of information, which is between 1 and 2 in a pair of measurements). Because TB_v and TB_h as observation pairs are correlated, DoI is below 2 and differences between TB_v and TB_h can become influenced by random instrument error. Thus, retrievals of SM and VOD by using two polarizations are not fully independent and errors can potentially affect one or both retrievals. The spurious noise reduces the robustness

of the method [22], [32]. For multiple angles, this effect is expected to be less pronounced due to the higher amount of information available [33], [34], although the depolarization with more dense vegetation will still reduce the amount of information across the angles. Also, note that other error sources are present, for example, from errors in the assumptions about the roughness parameter (h, e.g., [35], [36], [37]) and single-scattering albedo (ω). They are explored only complementarily in this work because our main focus here is on how TB errors impact SM and VOD.

To overcome these issues, SMAP-based VOD–SM retrievals have introduced various regularization approaches that aim to reduce retrieval noise by incorporating *a priori* information mainly about variations in VOD. The multitemporal DCA (MTDCA) is based on the premise that changes in the vegetation biomass occur on time scales that are longer than SM fluctuations due to storms and interstorms [32], [38]. Based on this assumption, the MTDCA uses two consecutive overpasses to retrieve two SM values and a single VOD output for each time-adjacent overpass pair. It also uses model selection over the entire record to estimate the effective single-scattering albedo as a static feature of the dominant vegetation type. Hence, four TB values (two for each overpass) are available to retrieve three unknowns. This increases DoI above three [32], [39]. As DoI is the upper limit on the number of possibly retrieved parameters, the problem is not necessarily overdetermined. This procedure results in two VOD values retrieved for each overpass (one using information from the overpass before and one using information from the overpass after). In averaging these two VOD values together, information from multiple overpasses ultimately constrains the VOD retrieved at a given overpass. Recently, other algorithms have also included time aggregation with *a priori* decision of the degree of regularization: the SMOS L3 algorithm [40] and the constrained multichannel algorithm (CMCA) [28]. These approaches often incorporate a penalty on time rates of change of VOD [29], [41]. Following a similar concept, new SMAP L3 dual-channel algorithm (L3-DCA) retrievals [26], [42] incorporate a Tikhonov regularization [43]. Despite being called a DCA, its incorporation of a regularization approach is at odds with traditional DCA approaches. For clarity, we refer to this DCA approach as L3-DCA throughout this article. This approach instead imposes a weighted *a priori* VOD based on the moderate resolution imaging spectroradiometer (MODIS) normalized difference vegetation index (NDVI) and penalizes deviations of the SMAP-retrieved VOD from this assumed time series. The retrieved VOD is therefore constrained by a less noisy, NDVI-based VOD seasonal climatology [26].

Despite these advances on new information metrics and regularization techniques, SMAP DCAs and regularization approaches still need to be evaluated. We recognize that the DoI metric is useful to quantify the information available in satellite measurements, but it does not uniquely indicate the robustness of the retrievals. For example, DoI may increase with more random noise (i.e., independent TB_v and TB_h values), which paradoxically suggests more robustness to noise. Therefore, here, we introduce an additional metric of retrieval susceptibility to noise (and hence robustness): the
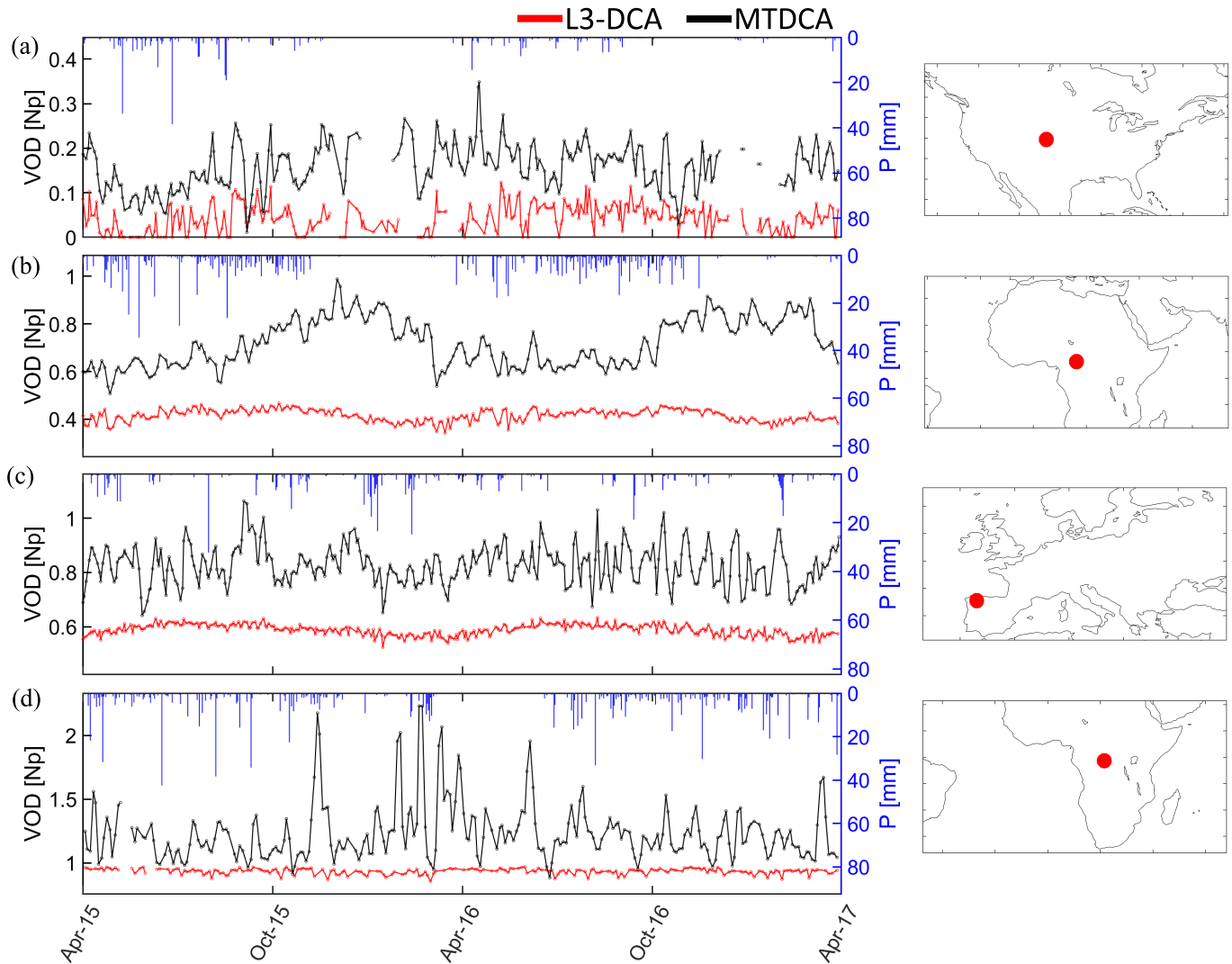
Fig. 1.   MTDCA VOD (black line) and L3-DCA VOD (red line) in (a) grasslands in central North America, (b) woody savanna in the Sahel, (c) deciduous forest in the northern Iberian Peninsula, and (d) tropical forests in the Congo basin. VOD data used in this figure are detailed in Section II-A. Precipitation estimates are based on the Global Precipitation Measurement (GPM) IMERG Final Precipitation L3 v06 product at 0.1 resolution [44]. Off-sets between the two VOD series are partially due to different algorithmic treatments of surface electromagnetic roughness and effective vegetation scattering albedo. Different behaviors in the two VOD products (i.e., smoother versus sharper changes along the time series) are likely due to the fact of using different regularization approaches which we investigate in this study.

signal-to-noise ratio (SNR). It complements DoI in order to provide a holistic understanding of the VOD retrieval algorithm robustness.

Regularization techniques can overconstrain the resulting VOD, thus removing VOD variability that contains a physical signal and creating an unwanted smoothing effect [29], [30]. We examine VOD from two common regularization techniques (Tikhonov for L3-DCA and multitemporal for MTDCA) at different time scales in order to gain an understanding of error sources and characteristics. Fig. 1 shows the examples that motivate this research. It shows time series of VOD from MTDCA and L3-DCA in several different vegetation conditions. Differences in VOD between the algorithms are likely due to the different regularization approaches that they use and to their different albedo (ω) and roughness (h) parameters. In low vegetation (grasslands), both VOD products have similar patterns in terms of variability [Fig. 1(a)].

Fig. 1(b) shows that seasonal variations in a woody savannah are captured by both approaches, but with a smaller L3-DCA seasonal amplitude. We aim to understand if either of the regularization approaches may be under or overregularizing the VOD variability both in seasonal and high-frequency variations. Fig. 1(c) and (d) show how high-frequency MTDCA VOD variation increases with biomass (i.e., the largest rapid changes are found in the tropical forest pixel), while the L3-DCA VOD time series is smooth in both cases (especially in the tropical forest). For dense vegetation, this motivates investigating whether the MTDCA approach may be carrying excess noise in its retrievals in high plant biomass regions. It also motivates determining whether the L3-DCA is overregularizing VOD variability, creating an unintended smoothing effect.

Therefore, in this study, we first assess the retrievability of VOD by examining observed $TB_v - TB_h$ differences and

using DoI and the proposed SNR. Second, we compare the VOD retrievals and noise of multitemporal and Tikhonov regularization techniques. We perform this test for both the full signal and the high-frequency signal near the Nyquist frequency. Our driving research questions are given as follows.

1) Which metrics quantify uncertainty in SM and VOD retrievals due to instrument noise and what do they reveal about current global SM–VOD retrievals?

2) How do the retrieved VOD time series based on commonly used regularization approaches qualitatively compare across different timescales of variability?

This work thus complements recent efforts to determine how TB error relatively propagates into SM and VOD in these algorithms, how much retrieved SM and VOD error is attributed to errors in the satellite measurements, radiative transfer model, and algorithmic parameterization, as well as how much VOD regularization reduces these errors [27], [29], [30], [45]. The assessment of these errors may have relevant implications as well for SM estimates, as the uncertainty in VOD is an important contributor to errors in SM retrievals [46, pp. 208–210], [47, Ch. 6].

II. DATA AND METHODS

A. Datasets

The SMAP mission was launched by the National Aeronautics and Space Administration (NASA) in January 2015. It has a native spatial resolution of ∼36 km (based on half power or −3-dB definition) and a revisit time of approximately 2–3 days depending on latitude. The following SMAP datasets are studied globally, using the descending passes of the satellite (6 A.M.) for the period April 2015–March 2020:

1) TBs at both vertical (TB_v) and horizontal (TB_h) polarizations from the L1C radiometer product, version 2 (SPL1CTB [49]). This product contains calibrated, geolocated TBs derived from SMAP Level-1B (L1B) antenna temperatures. Backus–Gilbert optimal interpolation methods are applied to extract maximum information from the antenna temperatures of SMAP and convert them to TBs at 9-km gridding (EASE2 grid).

2) The SMAP L3-DCA that contains SM, VOD, and constant albedo (ω) datasets. It is the SMAP-enhanced L3 radiometer SM product, version 4 (SPL3SMP [50]), also at 9-km gridding. It relies on the DCA algorithm to retrieve SM and VOD from the aforementioned L1C TBs. SM and VOD retrievals in this product are based on a Tikhonov regularization approach designed to remove excess noise in the VOD estimates, but at the cost of assuming an *a priori* VOD time series (see Section I). To do so, this method defines a degree of regularization, which modifies the least-squares misfit (χ^2) between modeled TBs (as a function of SM and VOD) and measured TBs. As such, this approach penalizes the retrieved VOD's deviation from the *a priori* VOD time series with the degree of penalty determined by an *a priori* multiplicative factor. Therefore, the regularization inputs information about VOD variations based on other time series such that the correlated TB

observations can be potentially used to reliably retrieve SM and VOD with reduced noise. More details on this regularization method are provided in [26] and [51].

3) The SMAP MTDCA SM, VOD, and ω datasets [38], [52]. Note that ω is constant for the study period. The product is also derived from the SMAP L1C 9-km TBs and applies the MTDCA retrieval algorithm for two consecutive overpasses. The algorithm is based on a time series method, which uses all TB values within a predefined time window. The default window length is two overpasses (i.e., 2–3 days depending on latitude). VOD is held constant between the two overpasses, but this is repeated for each time-adjacent overpass pair such that information from both time-adjacent overpasses is used (averaged) in the VOD retrieval. Therefore, the VOD variations, especially those due to noise, are reduced. Ultimately, this approach penalizes large changes in VOD between overpasses, eliminating noise more than the physical VOD signal [30].

In order to analyze the results, datasets on vegetation density and type are used. This includes the VWC product [42] that is used in the SCA. This VWC product is derived from NDVI seasonal climatologies from the NASA MODIS satellite for use within the SMAP algorithms. Complementarily, we also include the original MODIS NDVI [48]. In addition, land cover (LC) data from the MODIS International Geosphere-Biosphere Program (IGBP, MCD12C1 product v.6; 3-km resolution) is used to define homogeneous vegetation classes in two steps: 1) only the fully homogeneous 9-km pixels (i.e., those containing all 3-km pixels of the same LC class) are considered and 2) latitude and homogeneous LC pixels are applied to define seven different vegetation classes: tropical forests, temperate forests, boreal forests, savannahs, shrublands, grasslands, and croplands (Table S1, see the Supplementary Material).

B. $\tau - \omega$ Framework and Reliance on TB Polarization Differences

Retrievals of SM and VOD from passive microwave measurements rely on the inversion of a "zeroth-order" radiative transfer model, commonly known as the $\tau - \omega$ model [23]. In this model, the L-band TBs are represented as the sum of three terms: 1) the upwelling vegetation emission; 2) the downwelling emission from vegetation, which is reflected by the soil and then attenuated by the canopy; and 3) the direct soil emission and its attenuation through the vegetation

$$TB_p = (1 - \omega)(1 - \gamma)T_c + (1 - \omega)(1 - \gamma)\gamma$$
$$\cdot r_p \cdot T_c + (1 - r_p)\gamma \cdot T_s \quad (1)$$

where γ is the vegetation transmissivity, which depends on the VOD (algebraically represented by τ) according to Beer's law

$$\gamma = e^{\left(-\frac{\tau}{\cos\theta}\right)} \quad (2)$$

where θ is the incidence angle. Then, τ (used synonymously with VOD here) is one of the two unknowns to be retrieved. The VOD can be different for different polarizations. However, currently, neither the SMOS nor the SMAP science

data products account for any polarization difference; both assume that VOD is the same at both polarizations due to mixed orientation of vegetation at the 36-km scale. The soil reflectivity at polarization p (r_p) is linked to the soil dielectric constant through Fresnel equations and a nominal value of isotropic soil roughness. The soil dielectric constant is dependent on soil texture and SM. SM is the other unknown to be retrieved in the $\tau - \omega$ framework. The effective scattering albedo (ω) accounts for extinction and scattering effects due to vegetation. Albedo is obtained from nominal values distinguishing forest/nonforest vegetation in the case of the SMOS current algorithms [53, p. 2] and from lookup tables based on LC in the case of the SMAP ones (e.g., [42]). Like VOD, the albedo can have polarization differences that are not considered at this time. While efforts are underway to understand ω and its time dynamics [54], we focus only on SM and VOD retrievability here. T_c and T_s are the temperatures of the canopy and the soil, respectively. Both temperatures are assumed to be equivalent at SMOS and SMAP overpasses times (6 A.M. and 6 P.M. local times) and are obtained from ancillary surface temperature information. The isothermal assumption is known to hold well near 6 A.M. local time.

In dual-polarization algorithms, theoretically, VOD may be inferred alongside SM if there is observed TB polarization dependence above instrument noise. This is shown when separating out the polarization-dependent term (r_p) from (1)

$$\frac{\text{TB}_p}{T} = \gamma + (1 - \omega) \cdot (1 - \gamma) + \gamma\, r_p \big[(1 - \omega) \cdot (1 - \gamma) - 1 \big] \tag{3}$$

where the two values of surface reflectivity (r_p: one for TB_v and one for TB_h) will lead to two equations. In (3), the first term is the same for both polarizations (in the SMAP and SMOS implementations) and only the second term adds any polarization difference in the forward model. The joint retrievability of SM and VOD depends on a large enough difference in TB measurements at H and V polarizations. VOD is part of γ [see (2)]. If TB_v and TB_h approach one another, this suggests that the differences in r_h and r_v values are not making a large contribution to the emission as surface reflectivity typically has large differences at H and V polarizations. In this scenario, TB measurements have less contribution from the surface emission-influenced terms in the final bracketed term in (3), and thus, only VOD can be retrieved. However, this results in optimization instability when still attempting joint retrievals under this scenario [many combinations of possible SM and VOD would satisfy (3)]. Therefore, the robustness of DCAs is highly affected by the TB polarization difference fluctuations close to the instrument noise level, which can create noise in the estimations.

C. Analysis of the VOD Retrievability

To assess the VOD robustness, first, the relationship and differences between TB_h and TB_v are evaluated for different bins of VWC: 0–1, 3–4, and >9 kg/m^2. They represent three contrasting classes of vegetation density, ordered from lower to higher VWC (i.e., from lower to greater biomass):
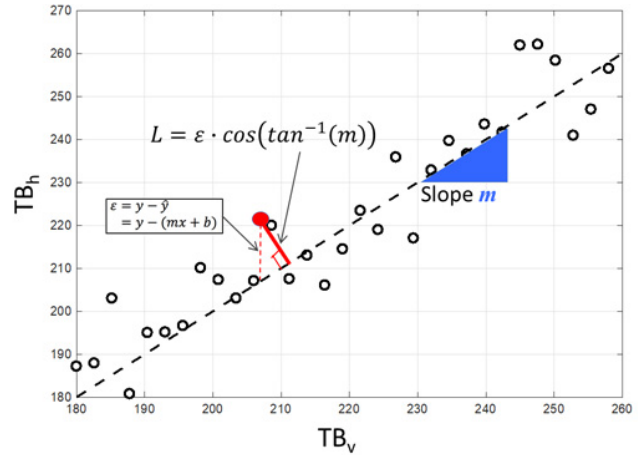

Fig. 2. Graphical summary of how the difference relative to the TB_v–TB_h linear dependence (L: red solid line) is computed.

1) low vegetation in semiarid regions, tundra, and steppes; 2) woodlands and nontropical forests; and 3) tropical forests (Fig. S1, see the Supplementary Material). This first analysis provides the broader context, which addresses how vegetation types reduce the TB_v–TB_h differences and, quantitatively, how close are they to the instrument noise.

Second, we use the DoI as proposed in [22]. DoI is a measure of how much independent information exists in several measurements (e.g., TB_v and TB_h) when the measurements are correlated. DoI is computed as

$$\text{DoI} = N - C_n(X_1, \ldots, X_n) \tag{4}$$

where N is the number of parameters (here, $N = 2$ if considering a single snapshot with TB_v and TB_h) and C_n represents the total correlation among the different parameters X_1–X_n (here, TB_v and TB_h). The total correlation is a generalization of the mutual information, which consists of the Kullback–Leibler divergence between the joint and the marginal entropies of the datasets. C_n captures the amount of information shared between any of the measurements in a set [22], [55]. Higher total correlation suggests less independent information between two parameters.

Third, we introduce an SNR metric to quantitatively assess retrievability. It measures how much TB_v and TB_h (two correlated measurements) are different relative to the instrument noise. The dispersion (standard deviation) of the polarization difference relative to the TB_v–TB_h linear dependence is computed. In Fig. 2, this polarization difference is distance L and is represented by a red solid line.

Once $\sigma(L)$ is obtained, then the SNR metric is

$$\text{SNR} = \frac{\sigma^2(L)}{\left(\text{NEDT}_v^2 + \text{NEDT}_h^2\right)} \tag{5}$$

where NEDT states for noise equivalent delta temperature for the L1C TBs, which is the measurement of the instrument noise. NEDT equals 0.77 according to the L1C TBs Assessment Report [51, p. 43]. The value is estimated over a stable vicarious target or constant temperature and salinity
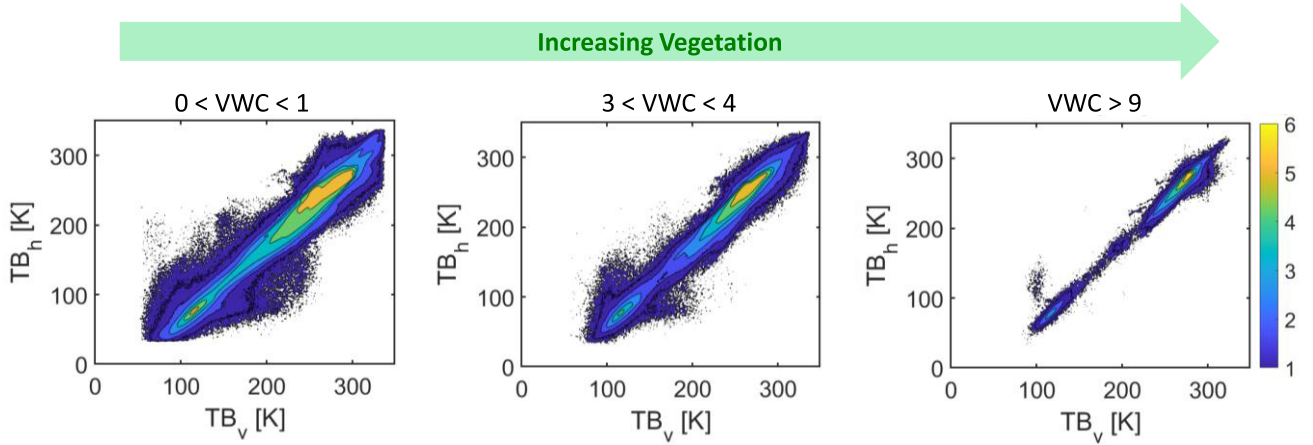
Fig. 3. Comparison of SMAP TBs at vertical (TB$_v$: x-axis) and horizontal (TB$_h$: y-axis) polarizations for increasing VWC: (Left) 0–1 kg/m^2, (Center) 3–4 kg/m^2, and (Right) >9 kg/m^2. See Fig. S1 for a map of the global distribution of the three categories. The color bar shows the density of pixels (decimal logarithm of the number of pixels).
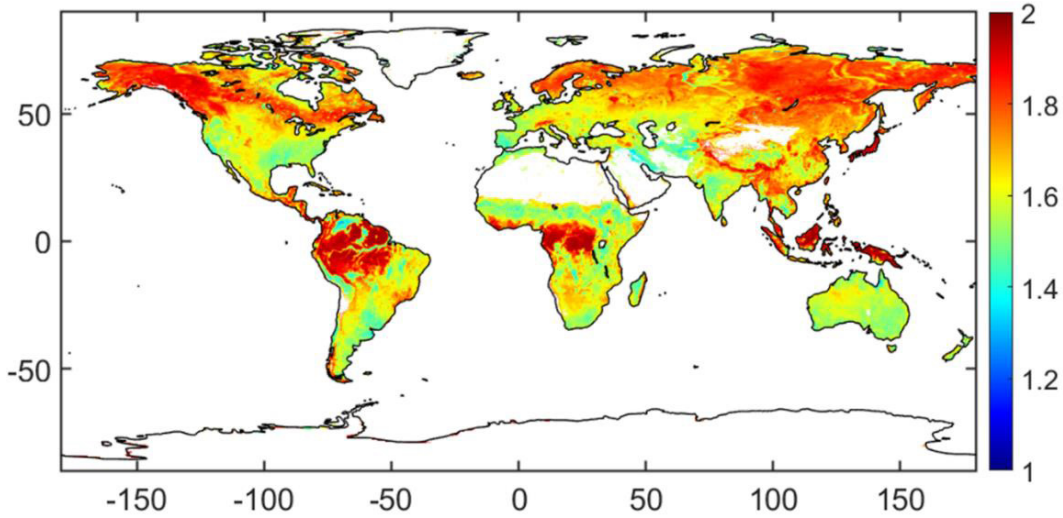

Fig. 4. DoI for TBs at vertical (TB$_v$) and horizontal (TB$_h$) polarizations. DoI measures how much independent information exists in several measurements (here two) when they are correlated (e.g., DoI = 1.5 indicates that 1.5 parameters may be retrieved).

ocean patches. Here, the NEDT of vertical and horizontal polarizations is assumed to be independent.

D. Metrics to Interpret the Effect of Regularization on VOD and Noise

Regularization techniques can mitigate issues of correlated TB$_v$ and TB$_h$ measurements. However, there are different regularization approaches that have produced satellite VOD retrievals and their differences have not been assessed. The SMAP L3-DCA VOD uses the Tikhonov regularization

$$\min_{X=\text{VOD,SM}} J = \sum_{p=H,V} \left(\text{TB}_{p\text{Obs}}(X) - \text{TB}_{p\text{Mod}}\right)^2$$
$$+ \lambda^2 \left(\text{VOD}_t - \text{VOD}_{\text{prior}_t}\right)^2 \quad (6)$$

where for a given overpass, VOD is retrieved simultaneously as in the traditional DCA (first addend), but a penalty (λ) is placed on VOD deviations from a prior input VOD based on NDVI climatology (second addend). This VOD prior input was

previously used in the SMAP SCA SM retrievals. A larger λ value would force the retrieved VOD to be closer to the VOD prior. By contrast, the MTDCA uses time-adjacent overpasses assuming that VOD is constant between n overpasses ($n = 2$ in the studied product, see Section II-A)

$$\min_{X=\text{VOD,SM}_1,\text{SM}_2} J = \sum_{t=1}^{n=2} \sum_{p=H,V} \left(\text{TB}_{p\text{Obs}}(X) - \text{TB}_{p\text{Mod}}\right)^2. \quad (7)$$

To evaluate the impacts of multitemporal and Tikhonov regularizations on the resulting VOD and noise, both the MTDCA and the L3-DCA products will be assessed and compared at different time scales. Results will be interpreted in the context of DoI and SNR. First, the mean annual VOD and the seasonal amplitude of the raw VOD signal are estimated and compared between the products. Second, the near-Nyquist frequency of VOD (NyVOD) and SM (NySM) will be computed by subtracting the seven-day moving averages from both raw variables. The high-frequency changes in
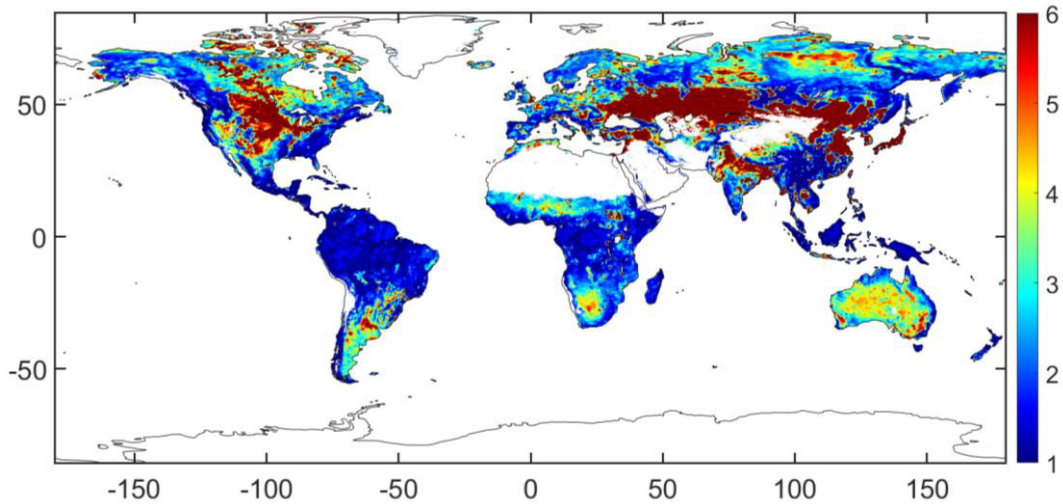
Fig. 5. Map of SNR, which is based on $\sigma(L)$. SNR provides a new metric to evaluate the robustness of VOD retrievals.
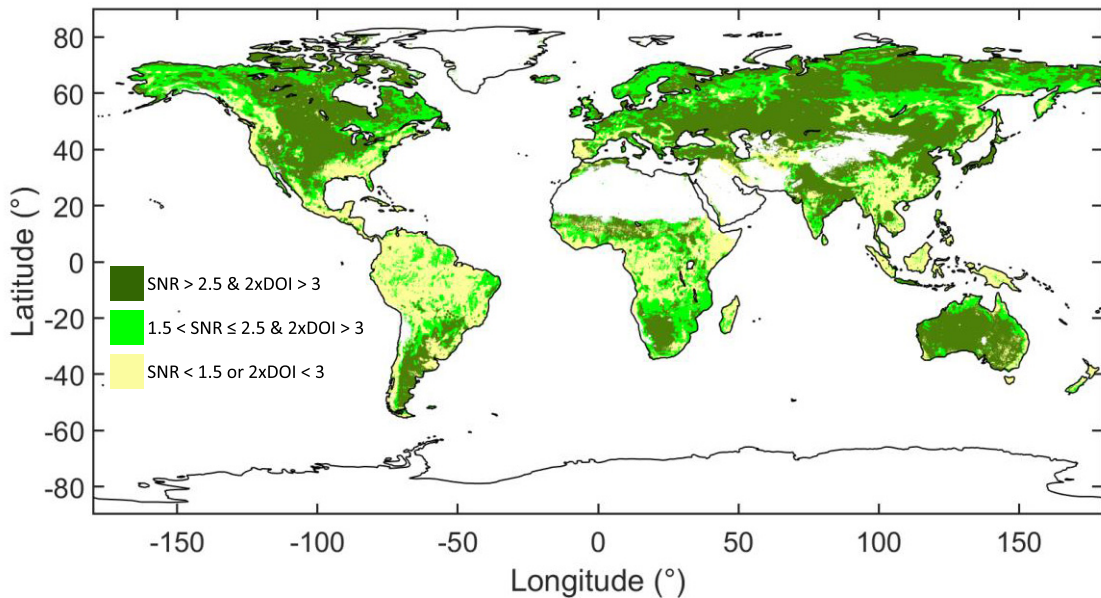

Fig. 6. Summary map of uncertainty of joint SM and VOD retrievals with regularization based on SNR and DOI. Dark green (higher confidence) spans 44.2% of global vegetated land, light green (medium confidence) spans 24.2%, and light yellow (lower confidence) spans 31.6%. DOI∗2 represents the degrees of information of two overpass pairs (or four TB measurements), which should be greater than 3 to be able to retrieve VOD without being an underdetermined problem. We use DOI∗2 here (instead of DOI) for a clearer interpretation of the retrievability, especially in the multitemporal case.

VOD will be analyzed by means of the standard deviation of the NyVOD. This will provide insight into the amount of remaining high-frequency VOD variations after regularization. Third, the covariance between NyVOD and NySM will be calculated in order to understand the influence of SM–VOD compensation occurring with noisy inputs during inversion and differences in this coupling between the two products. These results will be discussed in the context of SNR and SM–VOD retrieval errors compensation.

Note that VOD differences between algorithms will not solely be a function of the differences in regularization approaches in (7) and (8) because both approaches have different algorithmic choices, mainly in scattering albedo

and roughness parameters. Though we aim to address our second research question focusing on the aforementioned regularizations (which are commonly used in VOD studies), we also conduct complementary analyses on the impact of different albedos in the VOD differences between algorithms. In addition, we discuss the role that roughness may have on these differences.

III. RETRIEVABILITY OF VOD ACCORDING TO DOI AND SNR METRICS

The capacity of the $\tau-\omega$ framework to provide accurate VOD retrievals depends on the availability of at least two independent pieces of information. However, Fig. 3 shows
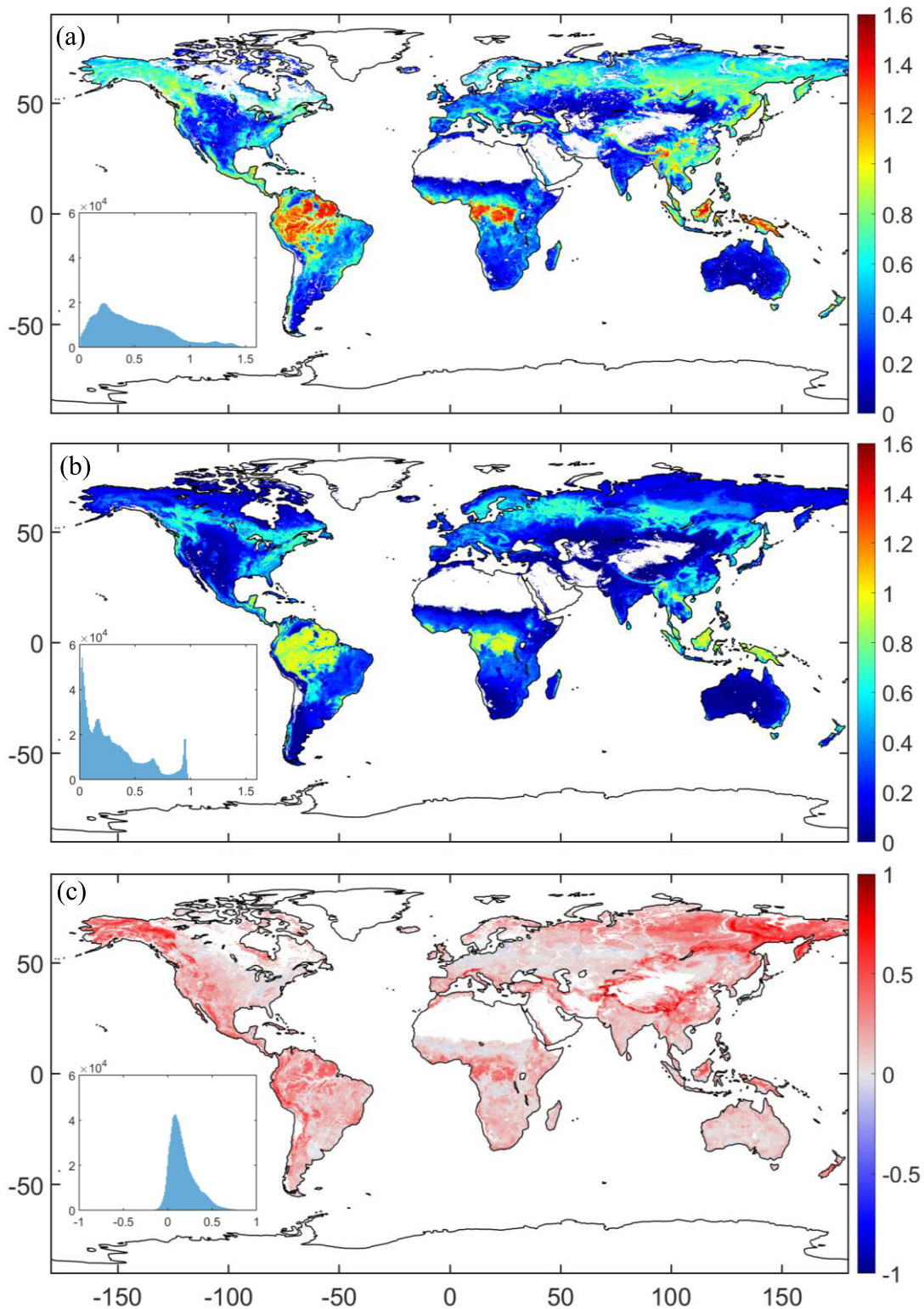
Fig. 7. (a) Mean of VOD retrieved with MTDCA, (b) mean of VOD retrieved with L3-DCA, and (c) differences between VOD retrievals (MTDCA − L3-DCA).

that TB_v and TB_h are highly correlated. Indeed, the TB_v–TB_h difference narrows as VWC increases [see (2) and (3)]. In the densest canopies where VWC > 9 kg/m^2 (i.e., tropical forests, Figs. 3 and S1) and NDVI > 0.8 (Fig. S2), the differences and their variability become small. This illustrates why TB_v and TB_h do not represent two independent data sources (Fig. 3) and their differences can be dominated by instrument error. In contrast, regions with less vegetation density (VWC < 1, i.e.,
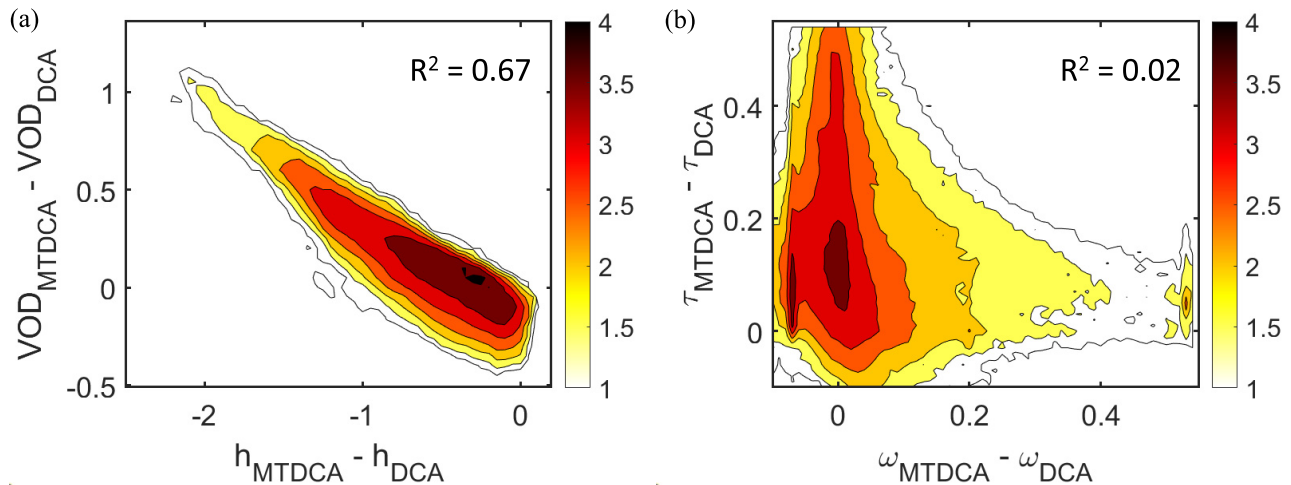
Fig. 8. Differences in VOD climatology between algorithms are compared to (a) differences between algorithm roughness parameter (h) and (b) differences in albedo (ω). The color bars show the decimal logarithm of counts. Roughness parameter differences explain nearly 70% of the mean bias in VOD from each algorithm. The scattering albedo has only a minor impact.

semiarid regions, see Fig. S1) do show larger differences and variations between vertical and horizontal polarizations (Fig. 3). This eases the partitioning between SM and VOD in the retrieval approaches as demonstrated with (3).

The DoI metric can be used to quantify the amount of independent information in the two measurements. Fig. 4 shows the DoI map where, generally, DoI ranges between 1.5 and 1.8 for two polarizations in many regions. Hence, theoretically, around 1.5 parameters can be inferred with a single satellite overpass (i.e., there is approximately 1.5 independent information content in TB_v and TB_h). In the case of multitemporal retrievals, the number of parameters that can be inferred should be (theoretically) the result of multiplying DoI by the number of overpasses (e.g., roughly three parameters for two consecutive samples [32]).

Nevertheless, DoI needs to be interpreted with caution as it may give "false positives" in very dense canopies if it is not interpreted in the context of noise. In particular, Figs. 4 and S3 show that DoI is very close to 2 in dense tropical forests (i.e., the Amazon, the Congo basin, and Indonesia). This is because noise dominates the signal in these dense vegetation regions. Variations in TBs are small or comparable to instrument noise. Hence, DoI is essentially measuring the independence of two uncorrelated time series. It suggests that there is enough independent information to retrieve two unknowns but does not consider that the variations are dominated by instrument noise rather than physical signal. This results in a deceiving DOI value of 2 for the pair. The polarization due to surface reflectivity (3) is largely attenuated: TBs are depolarized (Fig. 3), suggesting that only the instrument noise might be present in the measurements.

Thus, there is a need for an additional SNR metric to interpret the retrievability where the fluctuations in TB approach the instrument noise level. We introduce an SNR metric to complement the DoI in interpreting VOD retrievability. The SNR should measure, in the context of instrument noise, the ratio of signal to noise present after linearly predicting one covariate from another.

Fig. 5 shows the map of SNR. SNR values are close to 1 in dense tropical forests (median SNR = 1.24). This indicates that the signal is greatly influenced by noise and suggests caution in interpreting DoI alone. A low SNR shows that DoI is likely only higher in tropical forests because the total correlation is low due to noise. This quantifies the problem and shows, geographically precise, where retrievals of VOD may be problematic (Figs. 4 and 5). In other forest types, as well as in savannas, the value of DoI decreases and the SNR increases compared to tropical forests (median DoI and SNR in temperate forests: 1.72 and 1.44, respectively; median DoI and SNR in savannas: 1.60 and 1.71, respectively; Fig. S3). In the case of boreal forests, a higher SNR is found (median SNR = 2.24). Overall, this shows that VOD and SM retrievals based on DCAs should be robust in terms of available information in most land regions, including nontropical forests.

In contrast, lightly vegetated, nonforested regions have the largest variations in the difference in horizontal and vertical polarization TBs (Fig. 3). As shown in Figs. 5 and S3, this results in SNR values over 3 in semiarid regions (e.g., the Sahel and central Australia), grasslands (e.g., Central Asia, the U.S. Great Plains, and the Pampas), and croplands (e.g., the U.S. Corn Belt, Ukraine, Argentina, and the SW and SE areas of Australia). In these areas, the low vegetation density permits a good retrievability with high SNR, but in need of regularization as shown by DoI values closer to 1.5 (Figs. 4 and S3). Hence, VOD and SM retrievals will be achievable where DoI and SNR are both high. However, based on these SMAP measurements, DOI is well below 2 where SNR is high, meaning that some degree of regularization is needed to stabilize retrievals. DoI can be adjusted with regularization. However, SNR is intrinsic to the satellite measurements and thus cannot be directly altered. Therefore, we anticipate retrieval difficulty of VOD in wooded regions with low SNR, but an improvement on VOD retrievals after regularization in grasslands, croplands, and shrublands as well as in few cases of boreal and temperate forest areas (Figs. 6 and S3).
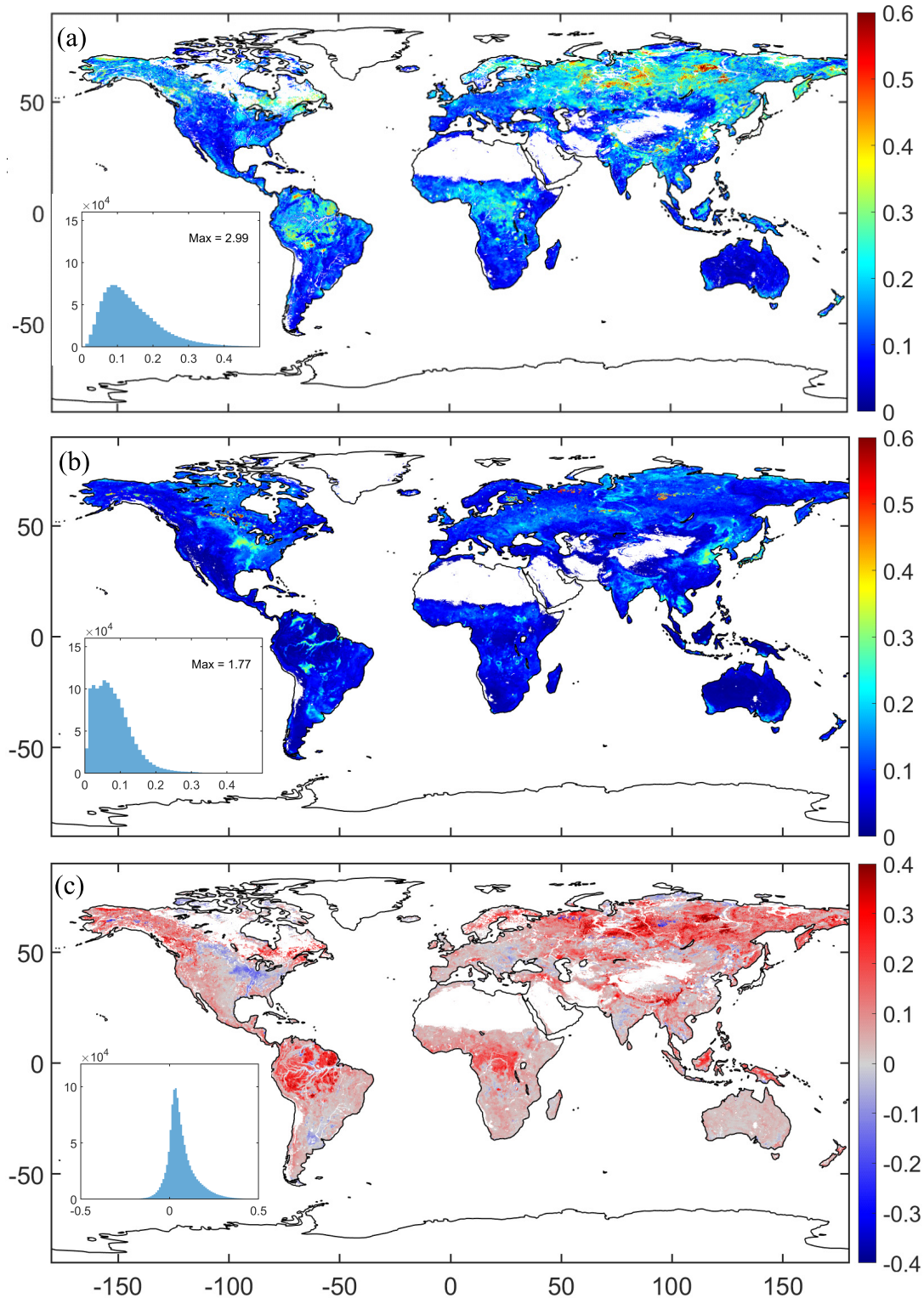
Fig. 9. Seasonal amplitudes of (a) MTDCA VOD and (b) L3-DCA VOD. (c) Differences between seasonal amplitudes (MTDCA − L3-DCA).

Taken together, DoI and SNR metrics suggest that VOD can be robustly retrieved with regularization in regions with low and moderate vegetation density with an increase in uncertainty in most savannas and forests, especially in tropical ones (Fig. 6). If DoI is doubled in a regularization approach (see Section IV), in regions where SNR is also high, both SM and VOD can be retrieved with lower risk of estimation instability within the optimization (Fig. 6). Fig. 6 should be used as a guide in determining where dual retrievals of SM and VOD are most certain using regularization approaches.
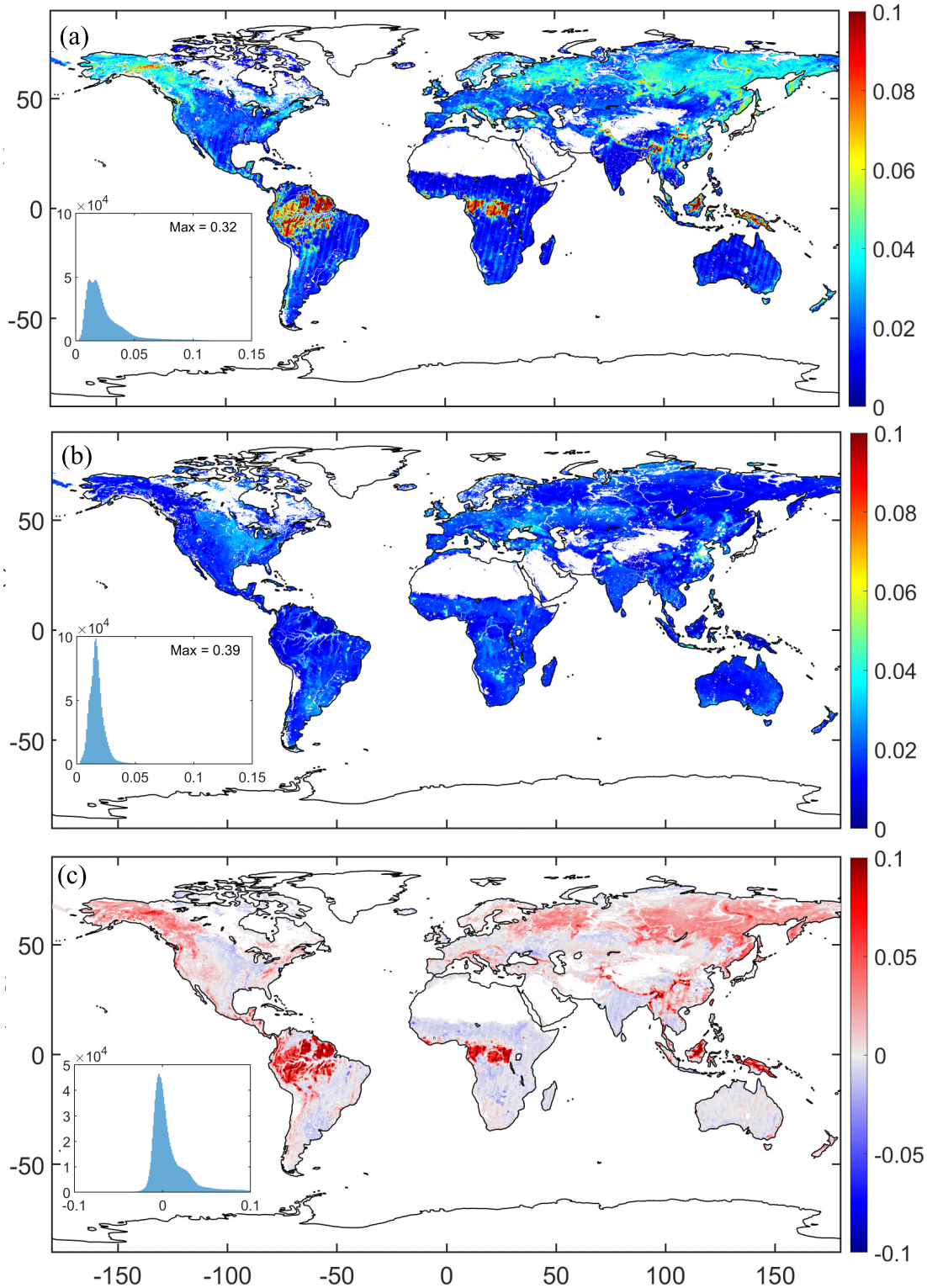
Fig. 10. Standard deviation of VOD at the Nyquist frequency for (a) MTDCA and (b) L3-DCA. (c) MTDCA minus the L3-DCA VOD standard deviation at the Nyquist frequency.

IV. IMPACTS OF TIKHONOV AND MULTITEMPORAL REGULARIZATIONS ON VOD RETRIEVALS AND NOISE

Global patterns of time-mean total VOD signal are shown in Fig. 7 for MTDCA (multitemporal regularization) and L3-DCA (Tikhonov regularization). The spatial patterns are similar, with Pearson's correlation coefficient (r) equal to 0.89, although mean VOD values for MTDCA are generally higher than those for L3-DCA (Fig. 7). These differences are partially attributable to choices of the roughness parameter (h)

in both algorithms, where higher h inputs generally reduce mean VOD. In particular, differences in h explain 67% of variance of the difference between the average VODs of both products [Fig. 8(a)], where lower L3-DCA's mean VOD can be partially explained by its higher h inputs. Again, note that the L3-DCA includes the SMAP product with Tikhonov regularization and is not a traditional DCA snapshot retrieval. In addition, note that we have found no relationship between differences in average VOD and those in ω [Fig. 8(b)].

The components of VOD variability at low frequency (i.e., seasonal amplitude) are shown in Fig. 9. Note that since the L3-DCA is constrained by NDVI climatology, the seasonal amplitude may partially be driven by the NDVI climatology amplitude and/or spatial pattern of conversion factors to VOD. The seasonal amplitudes are broadly comparable ($r = 0.44$), but the MTDCA shows slightly higher amplitudes, especially in forests [Fig. 9(c)]. This is expected because: 1) the L3-DCA's NDVI climatology prior will suppress any VOD interannual variability and 2) NDVI signal saturates for closed canopies and more dense vegetation [56], thus placing a maximum on the NDVI-based climatology used in L3-DCA regularization. We suggest that these considerations may be dampening the seasonal amplitude of L3-DCA VOD. A particular exception is croplands, where the seasonal amplitude is larger for the L3-DCA product than for MTDCA. This is evident in the U.S. Corn Belt and in crop areas of Argentina [Fig. 9(c)]. We suggest that time-based regularization approaches without an *a priori* VOD (such as the MTDCA) may have reduced capacity to capture the rapid growing phase seasonality and sharp amplitude in these regions; rapid corn growth may cause large VOD changes (around 0.2 Np) in less than ten days that VOD regularization approaches could dampen [41]. In the case of the Tikhonov regularization, accounting for an *a priori* VOD climatology may ease capturing a larger seasonal amplitude in these croplands, but at the cost of constraining changes in the retrievals between years, thus introducing interannual biases when studying crop phenology. In that sense, note that the large interannual variability of VOD in croplands (see [18, Fig. 6]) will be less detected by the L3-DCA VOD [55] because the *a priori* VOD is prescribed based on a constant mean NDVI climatology. The MTDCA may be better able to detect the interannual variability.

Overall, the difference in seasonal amplitudes may originate from both regularization approach differences as well as other parameter choices. For example, the magnitude of effective single-scattering albedo (ω) scales the impact of VOD on the TB. However, we find that these seasonal amplitude differences are not linked to the changes in ω between algorithms (results not shown) consistently with differences in mean VOD not being linked to changes in ω neither [Fig. 8(b)]. Instead, similar to the differences in VOD time means, a generally larger h roughness parameter chosen for the L3-DCA [Fig. 8(a)] and the use of an NDVI-based seasonality likely contribute to decrease the L3-DCA VOD seasonal variability in comparison to that of MTDCA.

We now evaluate the higher frequency variability near the Nyquist frequency (periods of 4–7 days for SMAP), which is
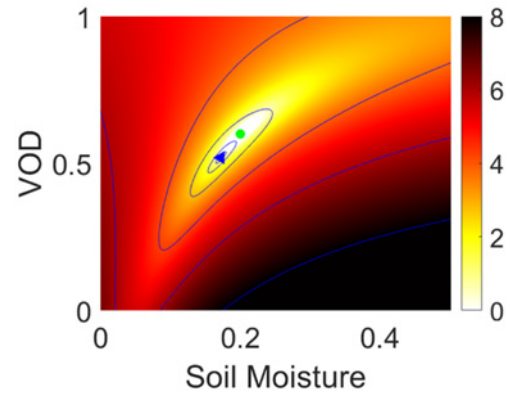

Fig. 11. DCA estimation cost function using synthetic data. The blue symbol is the true solution, while the green symbol is the noisy solution when the TB error on the order of 1 K is added to the measurements. Adapted from [27, Fig. 1].

more sensitive to noise, but the robustness of which can be improved through regularization [30]. The Nyquist variability removes some of the influence of the NDVI climatology prior, and thus, the L3-DCA NyVOD results are more of a function of the degree of regularization choice (λ). Fig. 10(a) and (b) show the standard deviation of the MTDCA and L3-DCA high-frequency values. A pattern emerges, which provides insight into how retrievable VOD is under different regularization approaches. The variability of MTDCA NyVOD is higher than that of L3-DCA NyVOD distinctly in tropical and boreal forests. Outside of these forests and in croplands, the NyVOD standard deviation tends to be lower for both algorithms. This implies that the forest biomes need additional constraints on VOD than the TBs alone can provide (such as an input VOD climatology), even with multitemporal persistence assumptions.

The estimation of the covariance between SM and VOD high-frequency variabilities provides insights into how much compensation may be taking place in inverting for SM and VOD simultaneously. Fig. 11 shows a representation of the joint VOD–SM cost function for an example of a dual-channel retrieval problem without regularization for a given overpass. In this example, the cost function has an elongated valley. Small amounts of noise will result in variations in retrievals following the contours of the valley. In the presence of noise, this compensation will result in positive covariance at the Nyquist frequency as shown by the positive VOD–SM relationship at the minimum cost function values (Fig. 11).

Given that SM and VOD errors are typically positively correlated (Fig. 11 and [30]), we evaluate systematic compensation between VOD and SM by computing the covariance between the SM and VOD at the Nyquist frequency. If the problem is significantly underdetermined, this may manifest itself as random variability (and thus as positive covariance) in the signal at high frequencies.

Fig. 12 shows the resulting covariance between VOD and SM at the Nyquist frequencies for each product. The covariance rather than the correlation is used to normalize out differences between the L3-DCA's and MTDCA's SM–VOD coupling that are due to the standard deviations of SM
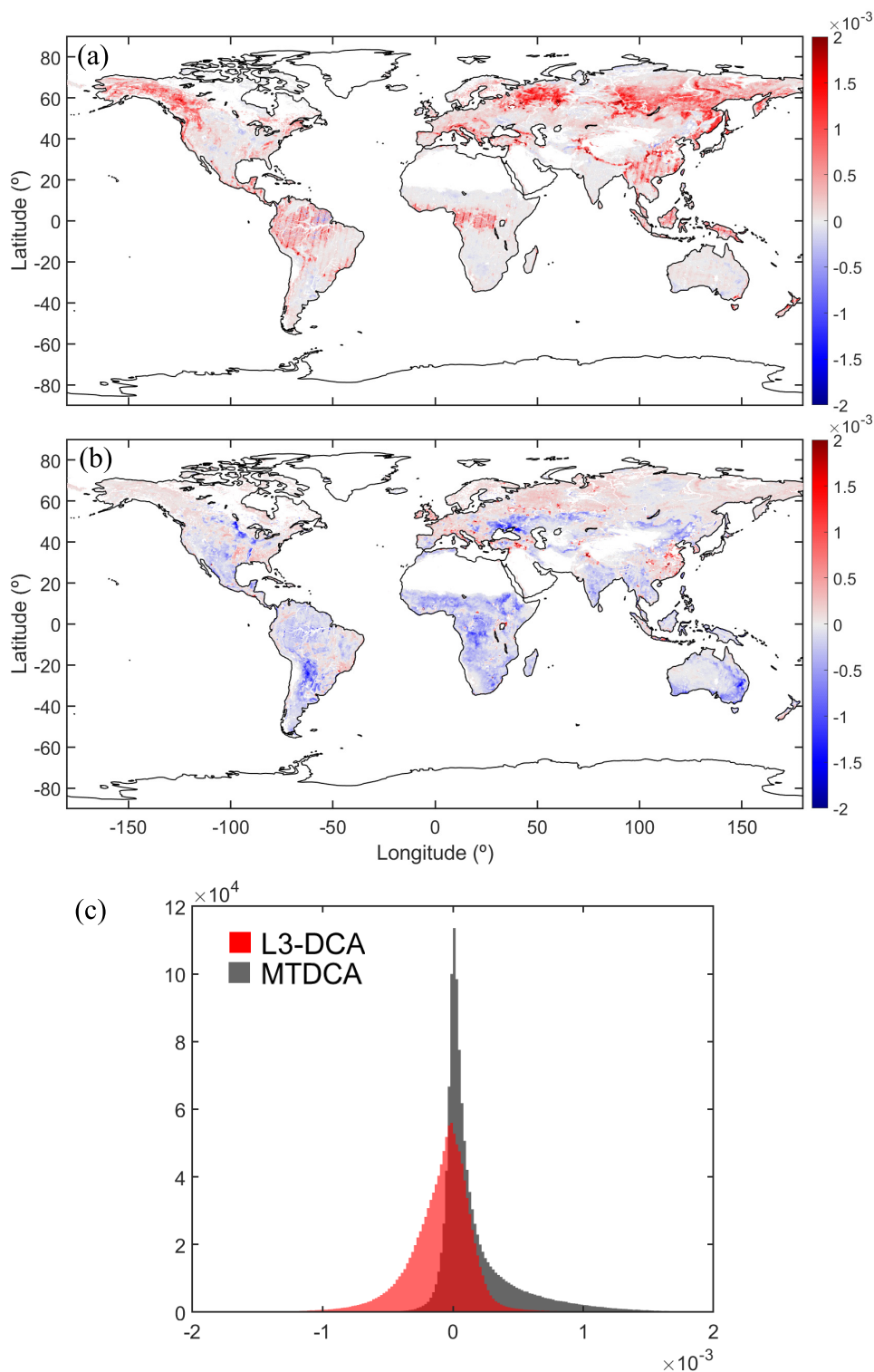
Fig. 12. (a) Map of covariance between Nyquist SM and Nyquist VOD for MTDCA. (b) Map of covariance between Nyquist SM and Nyquist VOD for L3-DCA. (c) Histogram comparing the distribution of covariances between Nyquist SM and Nyquist VOD for L3-DCA (red) and MTDCA (gray).

and VOD. For the multitemporal regularization (MTDCA), this covariance is positive on average [mean cov = 1.75×10^{-4}, see Fig. 12(a) and (c)]. This trend occurs in forest vegetation classes (Fig. S4, see the Supplementary Material). Importantly, these results indicate that the multitemporal

algorithm using two satellite overpasses may still be contaminated by errors. However, note that there are cases where positive covariance between SM and VOD on subweekly timescales is expected based on predawn soil–plant equilibrium under the plant hydraulic theory [15]. This may be the
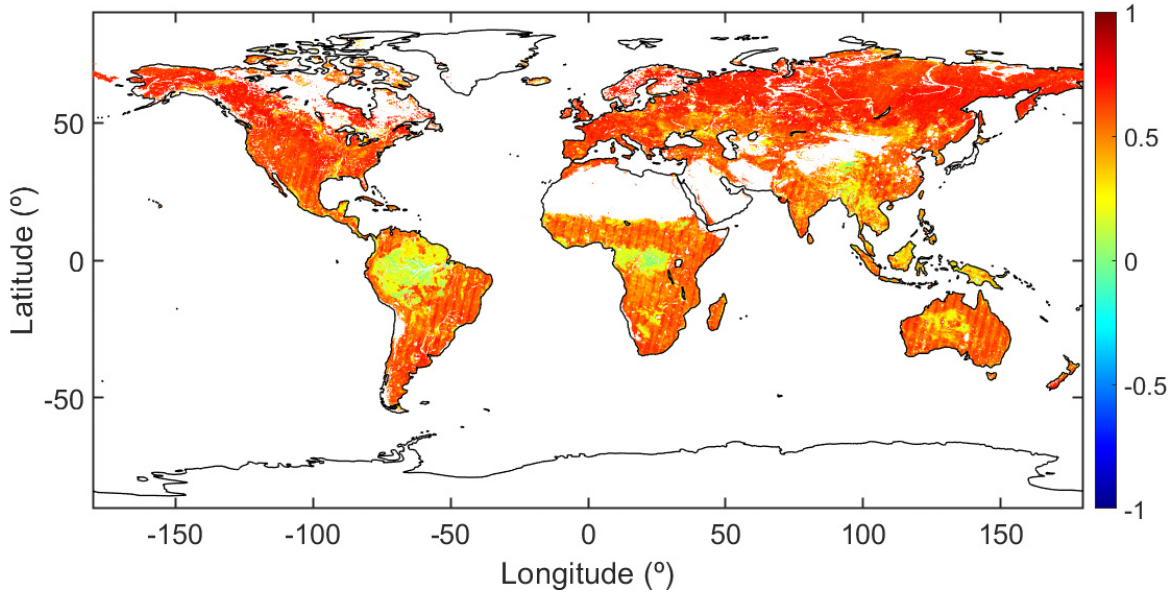
Fig. 13. Map of Pearson's correlation coefficient (r) between Nyquist VOD for MTDCA and Nyquist VOD for L3-DCA.

case in boreal forests, where the high covariance values for this vegetation class (Fig. S4) should not be related to VOD–SM compensation due to errors, as suggested by the high SNR in boreal woodlands (SNR > 2, see Figs. 5 and S4). It should be noted that forested regions with low SNR do show typically positive covariance, which may indicate mainly the effects of noise. In nonforest regions, where SNR is higher, the MTDCA shows low SM–VOD covariance at the Nyquist frequency. This is consistent with lack of SM–VOD compensating errors when retrievability is high. Also, negative covariance could be expected in semiarid regions, where negative SM–VOD correlation at short timescales occurs during dry-downs [16]. This is likely not observed here to as large of a degree as in previous work because we are analyzing the entire time series, not only dry-downs (Figs. 12 and S4).

For the Tikhonov regularization (L3-DCA product), the NySM-NyVOD covariance is slightly negative [mean cov = -1×10^{-4}, see Fig. 12(b) and (c)]. This happens independently of the SNR values (Figs. 5, 12, and S4). The trend is consistent through most vegetation classes, except for temperate (cov $\sim$ 0) and boreal forests (cov > 0, see Fig. S4). The exact mechanism leading to the negative covariance is unclear. Potentially, this may result from the Tikhonov regularization having too high of a degree of regularization. This is likely given that the Tikhonov approach in the L3-DCA uses MODIS greenness climatology as a prior. As such, the L3-DCA constrains the ability to assess high-frequency VOD variability. Tests indicate that the L3-DCA closely relates to the prior input of NDVI climatology (SCA-VOD) in many places (Fig. S5a), supporting that too much regularization may have been applied in the L3-DCA VOD retrievals. In particular, the correlation between L3-DCA and SCA-VOD is high (median correlation > 0.6) in boreal and temperate forests and in croplands (Fig. S5b).

Despite differences in the algorithms and coupling with SM, the high-frequency variability of VOD from both products

tends to be positively correlated (except in tropical forests, see Fig. 13). This indicates that the aforementioned differences may be playing a larger role on the amplitude of variations across frequencies of the variations. Ultimately, the detection of increases and decreases in VOD generally tends to be similar and in phase.

V. CONCLUSION

This study evaluates the robustness of VOD retrievals based on SMAP horizontal and vertical polarization TB measurements in the context of instrument noise. The study also assesses how two different SMAP VOD regularization techniques impact this robustness. Toward these goals, first, an SNR metric is proposed to capture variability above instrument noise; it is used as a complementary metric to the DoI that measures the statistical independence of measurements. Second, VOD retrievals and noise from two different VOD regularization approaches using SMAP observations are qualitatively compared across different time scales (annual mean, seasonal amplitude, and high-frequency variability). Namely, the SMAP MTDCA and L3-DCA products are compared based on multitemporal and Tikhonov regularization techniques, respectively.

We show that VOD can be robustly retrieved with regularization in regions with lower vegetation density and with more uncertainty in regions with greater vegetation density. Regions with the highest DoI values correspond to high vegetation densities (i.e., tropical forests, VWC > 9 kg/m^2), but these values are inflated due to random noise. Moreover, SNR is low based on high TB$_v$–TB$_h$ correlations, which indicates that the VOD signal in tropical forests is highly impacted by noise due to TB depolarization. Therefore, interpreting DoI alone is misleading in dense vegetation areas: values of DoI $\sim$ 2 are due to random noise, which gives the false impression of having two independent TB sources. We conclude that DoI must

be interpreted along with SNR for a holistic understanding of VOD retrievability. In contrast, low-density vegetation areas show high SNR values, with DoI being close to 1.5. The latter indicates the need for regularization in order to achieve robust retrievals with enough independent information. Ultimately, Fig. 6 is a guide for where regularized joint retrievals of SM and VOD would produce the smallest errors.

The comparison of multitemporal (MTDCA) and Tikhonov (L3-DCA) regularization techniques shows that their magnitudes of high-frequency variability are similar, except for in tropical forests where the variability of MTDCA NyVOD is higher than that of L3-DCA NyVOD. Furthermore, both regularization techniques show generally similar spatial patterns of high-frequency coupling of SM–VOD, where covariance tends to be neutral or negative in regions with herbaceous vegetation. This is because regularization reduces noise-based positive correlations between NySM and NyVOD. However, the L3-DCA NySM-NyVOD covariance tends to be lower and more negative on average than that of the MTDCA, even in tropical forests. Based on the more negative NySM-NyVOD coupling and reduced VOD high-frequency variability with the L3-DCA product, we suggest that this may be due to too high of a degree of regularization imposed in the L3-DCA Tikhonov algorithm, which forces the VOD retrieval to be like the VOD *a priori* time series based on NDVI climatology. We provide evidence for this by showing that in many global regions, the L3-DCA VOD retrieval is still temporally similar to its VOD *a priori* constraint. This may overconstrain VOD variability in some cases. Conversely, the MTDCA may require an *a priori* VOD time series in tropical forests because regularization alone is insufficient to prevent high positive correlations between SM and VOD and high standard deviation of VOD likely due to noise. This indicates that potentially, a VOD *a priori* constraint via the Tikhonov regularization may only be needed in more densely vegetated regions. A more naïve approach such as the MTDCA or Sobolev-norm regularization that does not require an *a priori* VOD time series may be sufficient for regions with low-density vegetation.

Ultimately, the high-frequency signals of the L3-DCA and MTDCA VOD time series positively correlate (except for tropical forests). Therefore, despite the differences in VOD retrieval approaches and potential for underregularization and overregularization in each product, the increases and decreases in VOD at subweekly timescales are in phase between the algorithms. This indicates that the amplitude of variability across different frequencies may be more impacted than the subweekly detection of increases and decreases in VOD. More confidence may therefore be exhibited in the use of VOD to detect plant rehydration and water loss rather than the magnitude of these changes. These patterns emerge independent of the regularization approach.

Altogether, from the results presented here, we first recommend the simultaneous application of SNR and DoI metrics for the evaluation of VOD robustness. Second, we suggest further assessing whether the degree of regularization within the SMAP L3-DCA's Tikhonov approach is too high. If so, it can be reduced to capture VOD dynamics where

adequate polarization information exists based on TBs, DoI, and SNR. This reduction could be addressed by using a spatially varying λ (instead of a global constant value) according to a map of VOD noise [see [26, Fig. 2(a)]. Third, we recommend potentially increasing the regularization in the multitemporal retrievals or imposing *a priori* climatology for noise-dominated regions (mainly tropical forests). Also, future work should be addressed to evaluate the robustness of VOD retrievals for other algorithms (e.g., CMCA [28]) and sensors (the L3 algorithm of SMOS [40]), which are based on time-aggregation approaches using *a priori* regularization. We expect that the implementation of these changes can lead to more accurately retrieving SM–VOD dynamics.

REFERENCES

[1] D. Entekhabi *et al.*, "The soil moisture active passive (SMAP) mission," *Proc. IEEE*, vol. 98, no. 5, pp. 704–716, May 2010, doi: 10.1109/JPROC.2010.2043918.

[2] Y. H. Kerr *et al.*, "The SMOS mission: New tool for monitoring key elements of the global water cycle," *Proc. IEEE*, vol. 98, no. 5, pp. 666–687, May 2010, doi: 10.1109/JPROC.2010.2043032.

[3] T. J. Schmugge and T. J. Jackson, "A dielectric model of the vegetation effects on the microwave emission from soils," *IEEE Trans. Geosci. Remote Sens.*, vol. 30, no. 4, pp. 757–760, Jul. 1992, doi: 10.1109/36.158870.

[4] M. Momen *et al.*, "Interacting effects of leaf water potential and biomass on vegetation optical depth," *J. Geophys. Res., Biogeosci.*, vol. 122, no. 11, pp. 3031–3046, Nov. 2017, doi: 10.1002/2017JG004145.

[5] N. M. Holtzman *et al.*, "L-band vegetation optical depth as an indicator of plant water potential in a temperate deciduous forest stand," *Biogeosciences*, vol. 18, no. 2, pp. 739–753, Feb. 2021, doi: 10.5194/bg-18-739-2021.

[6] M. Brandt *et al.*, "Satellite passive microwaves reveal recent climate-induced carbon losses in African drylands," *Nature Ecol. Evol.*, vol. 2, no. 5, pp. 827–835, May 2018, doi: 10.1038/s41559-018-0530-6.

[7] L. Fan *et al.*, "Satellite-observed pantropical carbon dynamics," *Nature Plants*, vol. 5, no. 9, pp. 944–951, Sep. 2019, doi: 10.1038/s41477-019-0478-9.

[8] A. Mialon *et al.*, "Evaluation of the sensitivity of SMOS L-VOD to forest above-ground biomass at global scale," *Remote Sens.*, vol. 12, no. 9, p. 1450, May 2020, doi: 10.3390/rs12091450.

[9] D. Chaparro, M. Piles, M. Vall-Llossera, A. Camps, A. G. Konings, and D. Entekhabi, "L-band vegetation optical depth seasonal metrics for crop yield assessment," *Remote Sens. Environ.*, vol. 212, pp. 249–259, Jun. 2018, doi: 10.1016/j.rse.2018.04.049.

[10] A. Mateo-Sanchis, M. Piles, J. Muñoz-Marí, J. E. Adsuara, A. Pérez-Suay, and G. Camps-Valls, "Synergistic integration of optical and microwave satellite data for crop yield estimation," *Remote Sens. Environ.*, vol. 234, Dec. 2019, Art. no. 111460, doi: 10.1016/j.rse.2019.111460.

[11] S. Sadri, E. F. Wood, and M. Pan, "Developing a drought-monitoring index for the contiguous US using SMAP," *Hydrol. Earth Syst. Sci.*, vol. 22, no. 12, pp. 6611–6626, Dec. 2018, doi: 10.5194/hess-22-6611-2018.

[12] K. Rao, W. R. L. Anderegg, A. Sala, J. Martínez-Vilalta, and A. G. Konings, "Satellite-based vegetation optical depth as an indicator of drought-driven tree mortality," *Remote Sens. Environ.*, vol. 227, pp. 125–136, Jun. 2019.

[13] L. Fan *et al.*, "Evaluation of microwave remote sensing for monitoring live fuel moisture content in the Mediterranean region," *Remote Sens. Environ.*, vol. 205, pp. 210–223, Feb. 2018.

[14] M. Forkel, L. Schmidt, R. M. Zotta, W. Dorigo, and M. Yebra, "Estimating leaf moisture content at global scale from passive microwave satellite observations of vegetation optical depth," *Hydrol. Earth Syst. Sci. Discuss.*, pp. 1–43, Aug. 2022, doi: 10.5194/hess-2022-121.

[15] A. F. Feldman, D. J. Short Gianotti, A. G. Konings, P. Gentine, and D. Entekhabi, "Patterns of plant rehydration and growth following pulses of soil moisture availability," *Biogeosciences*, vol. 18, no. 3, pp. 831–847, Feb. 2021, doi: 10.5194/bg-18-831-2021.

[16] A. F. Feldman *et al.*, "Moisture pulse-reserve in the soil-plant continuum observed across biomes," *Nature Plants*, vol. 4, pp. 1026–1033, Dec. 2018, doi: 10.1038/s41477-018-0304-9.

[17] D. S. Lyons, S. Z. Dobrowski, Z. A. Holden, M. P. Maneta, and A. Sala, "Soil moisture variation drives canopy water content dynamics across the western U.S.," *Remote Sens. Environ.*, vol. 253, Feb. 2021, Art. no. 112233, doi: 10.1016/j.rse.2020.112233.

[18] B. K. Hornbuckle *et al.*, "SMOS optical thickness changes in response to the growth and development of crops, crop management, and weather," *Remote Sens. Environ.*, vol. 180, pp. 320–333, Jul. 2016, doi: 10.1016/j.rse.2016.02.043.

[19] K. Togliatti *et al.*, "Quantitative assessment of satellite L-band vegetation optical depth in the US corn belt," *IEEE Geosci. Remote Sens. Lett.*, vol. 19, pp. 1–5, 2022, doi: 10.1109/LGRS.2020.3034174.

[20] K. Togliatti *et al.*, "Satellite L–band vegetation optical depth is directly proportional to crop water in the U.S. corn belt," *Remote Sens. Environ.*, vol. 233, Nov. 2019, Art. no. 111378, doi: 10.1016/j.rse.2019.111378.

[21] Y. Zhang, S. Zhou, P. Gentine, and X. Xiao, "Can vegetation optical depth reflect changes in leaf water potential during soil moisture dry-down events?" *Remote Sens. Environ.*, vol. 234, Dec. 2019, Art. no. 111451, doi: 10.1016/j.rse.2019.111451.

[22] A. G. Konings, K. A. McColl, M. Piles, and D. Entekhabi, "How many parameters can be maximally estimated from a set of measurements?" *IEEE Geosci. Remote Sens. Lett.*, vol. 12, no. 5, pp. 1081–1085, May 2015, doi: 10.1109/LGRS.2014.2381641.

[23] T. Mo, B. J. Choudhury, T. J. Schmugge, J. R. Wang, and T. J. Jackson, "A model for microwave emission from vegetation-covered fields," *J. Geophys. Res., Oceans*, vol. 87, no. C13, pp. 11229–11237, Dec. 1982, doi: 10.1029/JC087iC13p11229.

[24] J.-P. Wigneron *et al.*, "Modelling the passive microwave signature from land surfaces: A review of recent results and application to the L-band SMOS & SMAP soil moisture retrieval algorithms," *Remote Sens. Environ.*, vol. 192, pp. 238–262, Apr. 2017.

[25] R. Bindlish, T. Jackson, M. Cosh, T. Zhao, and P. O'Neill, "Global soil moisture from the aquarius/SAC-D satellite: Description and initial assessment," *IEEE Geosci. Remote Sens. Lett.*, vol. 12, no. 5, pp. 923–927, May 2015, doi: 10.1109/LGRS.2014.2364151.

[26] J. Chaubell *et al.*, "Regularized dual-channel algorithm for the retrieval of soil moisture and vegetation optical depth from SMAP measurements," *IEEE J. Sel. Topics Appl. Earth Observ. Remote Sens.*, vol. 15, pp. 102–114, 2022, doi: 10.1109/JSTARS.2021.3123932.

[27] B. Li and S. P. Good, "Information-based uncertainty decomposition in dual-channel microwave remote sensing of soil moisture," *Hydrol. Earth Syst. Sci.*, vol. 25, no. 9, pp. 5029–5045, Sep. 2021, doi: 10.5194/hess-25-5029-2021.

[28] A. Ebtehaj and R. L. Bras, "A physically constrained inversion for high-resolution passive microwave retrieval of soil moisture and vegetation water content in L-band," *Remote Sens. Environ.*, vol. 233, Nov. 2019, Art. no. 111346, doi: 10.1016/j.rse.2019.111346.

[29] S. Zwieback, D. D. Bosch, M. H. Cosh, P. J. Starks, and A. Berg, "Vegetation–soil moisture coupling metrics from dual-polarization microwave radiometry using regularization," *Remote Sens. Environ.*, vol. 231, Sep. 2019, Art. no. 111257, doi: 10.1016/j.rse.2019.111257.

[30] A. Feldman, D. Chaparro, and D. Entekhabi, "Error propagation in microwave soil moisture and vegetation optical depth retrievals," *IEEE J. Sel. Topics Appl. Earth Observ. Remote Sens.*, vol. 14, pp. 11311–11323, 2021, doi: 10.1109/JSTARS.2021.3124857.

[31] L. Gao, A. Ebtehaj, M. J. Chaubell, M. Sadeghi, X. Li, and J.-P. Wigneron, "Reappraisal of SMAP inversion algorithms for soil moisture and vegetation optical depth," *Remote Sens. Environ.*, vol. 264, Oct. 2021, Art. no. 112627, doi: 10.1016/j.rse.2021.112627.

[32] A. G. Konings, M. Piles, K. Rötzer, K. A. McColl, S. K. Chan, and D. Entekhabi, "Vegetation optical depth and scattering albedo retrieval using time series of dual-polarized L-band radiometer observations," *Remote Sens. Environ.*, vol. 172, pp. 178–189, Jan. 2016, doi: 10.1016/j.rse.2015.11.009.

[33] R. Fernandez-Moran *et al.*, "SMOS-IC: An alternative SMOS soil moisture and vegetation optical depth product," *Remote Sens.*, vol. 9, no. 5, p. 457, May 2017, doi: 10.3390/rs9050457.

[34] J. P. Wigneron, P. Waldteufel, A. Chanzy, J.-C. Calvet, and Y. Kerr, "Two-dimensional microwave interferometer retrieval capabilities over land surfaces (SMOS mission)," *Remote Sens. Environ.*, vol. 73, no. 3, pp. 270–282, 2000, doi: 10.1016/S0034-4257(00)00103-6.

[35] J. P. Wigneron, L. Laguerre, and Y. H. Kerr, "A simple parameterization of the L-band microwave emission from rough agricultural soils," *IEEE Trans. Geosci. Remote Sens.*, vol. 39, no. 8, pp. 1697–1707, Aug. 2001, doi: 10.1109/36.942548.

[36] R. Panciera, J. P. Walker, and O. Merlin, "Improved understanding of soil surface roughness parameterization for L-band passive microwave soil moisture retrieval," *IEEE Geosci. Remote Sens. Lett.*, vol. 6, no. 4, pp. 625–629, Oct. 2009, doi: 10.1109/LGRS.2009.2013369.

[37] V. A. Walker, B. K. Hornbuckle, and M. H. Cosh, "Refining SMAP soil roughness parameterization in the U.S. corn belt," in *Proc. IEEE Int. Geosci. Remote Sens. Symp. (IGARSS)*, Yokohama, Japan, Jul. 2019, doi: 10.1109/IGARSS.2019.8898618.

[38] A. G. Konings, M. Piles, N. Das, and D. Entekhabi, "L-band vegetation optical depth and effective scattering albedo estimation from SMAP," *Remote Sens. Environ.*, vol. 198, pp. 460–470, Sep. 2017, doi: 10.1016/j.rse.2017.06.037.

[39] A. F. Feldman and D. Entekhabi, "Smap vegetation optical depth retrievals using the multi-temporal dual-channel algorithm," in *Proc. IEEE Int. Geosci. Remote Sens. Symp. (IGARSS)*, Yokohama, Japan, Jul. 2019, pp. 5437–5440, doi: 10.1109/IGARSS.2019.8899014.

[40] A. Al Bitar *et al.*, "The global SMOS level 3 daily soil moisture and brightness temperature maps," *Earth Syst., Sci. Data*, vol. 9, pp. 293–315, Jun. 2017, doi: 10.5194/essd-9-293-2017.

[41] L. Gao, M. Sadeghi, and A. Ebtehaj, "Microwave retrievals of soil moisture and vegetation optical depth with improved resolution using a combined constrained inversion algorithm: Application for SMAP satellite," *Remote Sens. Environ.*, vol. 239, Mar. 2020, Art. no. 111662, doi: 10.1016/j.rse.2020.111662.

[42] P. E. O'Neill *et al.*, "SMAP enhanced L2 radiometer half-orbit 9 km EASE-grid soil moisture, version 5 [data set]," NASA Nat. Snow Ice Data Center Distrib. Act. Arch. Center, Boulder, CO, USA, 2021, doi: 10.5067/LOT311EZHH8S.

[43] A. N. Tikhonov, "On the solution of ill-posed problems and the method of regularization," *Doklady Akademii Nauk*, vol. 151, no. 3, pp. 501–504, 1963.

[44] G. J. Huffman, E. F. Stocker, D. T. Bolvin, E. J. Nelkin, and T. Jackson "GPM IMERG final precipitation L3 1 day 0.1 degree × 0.1 degree V06," in *Goddard Earth Sciences Data and Information Services Center (GES DISC)*, A. Savtchenko, Ed. Greenbelt, MD, USA: Accessed: Dec. 1, 2021, doi: 10.5067/GPM/IMERGDF/DAY/06.

[45] J. Dong, W. T. Crow, and R. Bindlish, "The error structure of the SMAP single and dual channel soil moisture retrievals," *Geophys. Res. Lett.*, vol. 45, no. 2, pp. 758–765, Jan. 2018, doi: 10.1002/2017GL075656.

[46] A. A. Chukhlantsev, *Microwave Radiometry of Vegetation Canopies*, vol. 24. Heidelberg, Germany: Springer, 2006.

[47] F. T. Ulaby, R. K. Moore, and A. K. Fung, "Microwave remote sensing: Active and passive," in *From Theory to Applications* vol. 3. Artech House, 1986.

[48] K. Didan, "MOD13A2 MODIS/terra vegetation indices 16-day L3 global 1 km SIN grid V006 [data set]," NASA EOSDIS Land Processes DAAC, Tech. Rep., 2015, doi: 10.5067/MODIS/MOD13A2.006.

[49] M. J. Chaubell, J. S. Chan, R. S. Dunbar, J. Peng, and S. Yueh, "SMAP enhanced L1C radiometer half-orbit 9 km ease-grid brightness temperatures, version 2," NASA Nat. Snow Ice Data Center DAAC, Boulder, CO, USA, Tech. Rep., 2018, doi: 10.5067/0DGGEWUC6MLY.

[50] P. E. O'Neill, S. Chan, T. Jackson, R. Bindlish, and J. Chaubell, "SMAP enhanced L3 radiometer global daily 9 km ease-grid soil moisture, version 4," NASA Nat. Snow Ice Data Center DAAC, Boulder, CO, USA, Tech. Rep., 2020, doi: 10.5067/NJ34TQ2LFE90.

[51] S. Chan and R. S. Dunbar, "Enhanced level 1C radiometer data product specification document," Jet Propuls. Lab., California Inst. Technol., Pasadena, CA, USA, Tech. Rep., 2020, p. 55.

[52] A. Feldman, A. Konings, M. Piles, and D. Entekhabi, "The multi-temporal dual channel algorithm (MT-DCA)," Zenodo, Tech. Rep., Oct. 2021, doi: 10.5281/zenodo.5619583.

[53] Y. H. Kerr, P. Waldteufel, P. Richaume, I. Davenport, P. Ferrazzoli, and J. P. Wigneron, "SMOS level 2 processor soil moisture algorithm theoretical basis document (ATBD)," CBSA, UoR, TV and INRA, Toulouse, France, Tech. Rep. SO-TN-ARR-L2PP-0037, vol. 3, 2006.

[54] M. J. Baur, T. Jagdhuber, A. F. Feldman, D. Chaparro, M. Piles, and D. Entekhabi, "Time-variations of zeroth-order vegetation absorption and scattering at L-band," *Remote Sens. Environ.*, vol. 267, Dec. 2021, Art. no. 112726, doi: 10.1016/j.rse.2021.112726.

[55] S. Watanabe, "Information theoretical analysis of multivariate correlation," *IBM J. Res. Develop.*, vol. 4, no. 1, pp. 66–82, Jan. 1960, doi: 10.1147/rd.41.0066.

[56] D. Chaparro *et al.*, "Sensitivity of L-band vegetation optical depth to carbon stocks in tropical forests: A comparison to higher frequencies and optical indices," *Remote Sens. Environ.*, vol. 232, Oct. 2019, Art. no. 111303, doi: 10.1016/j.rse.2019.111303.

[57] V. A. Walker, B. K. Hornbuckle, M. H. Cosh, and J. H. Prueger, "Seasonal evaluation of SMAP soil moisture in the U.S. corn belt," *Remote Sens.*, vol. 11, no. 21, p. 2488, Oct. 2019, doi: 10.3390/rs11212488.

David Chaparro received the B.S. degree in biology from the Universitat Autònoma de Barcelona, Barcelona, Spain, in 2011, the M.S. degree in remote sensing and geographic information systems and the M.S. degree in terrestrial ecology from the Center for Ecological Research and Forestry Applications, Barcelona, in 2012 and 2013, respectively, and the Ph.D. degree in telecommunication engineering from the Universitat Politècnica de Catalunya, Barcelona, in 2018.

He is currently a Post-Doctoral Researcher with the Microwaves and Radar Institute, German Aerospace Center (DLR), Weßling, Germany. He is working on vegetation moisture retrievals from satellites and exploring new frameworks to study the soil–plant–atmosphere continuum from satellite sensor synergies. His research interests include Earth observation from microwave radiometers and optical sensors to develop environmental research and applications.

Andrew F. Feldman (Member, IEEE) received the B.S. and M.S. degrees in civil engineering from Drexel University, Philadelphia, PA, USA, in 2016, and the M.S. and Ph.D. degrees in civil and environmental engineering from the Massachusetts Institute of Technology (MIT), Cambridge, MA, USA, in 2018 and 2021, respectively.

He is currently a NASA Post-Doctoral Program Fellow with the Biospheric Sciences Laboratory, NASA Goddard Space Flight Center, Greenbelt, MD, USA. His research interests include land-surface hydrology, terrestrial ecosystem science, and microwave remote sensing.

Mario Julian Chaubell received the Bachelor of Science degree in mathematics from the University of Mar del Plata, Buenos Aires, Argentina, in 1997, and the Ph.D. degree in applied and computational mathematics from the California Institute of Technology, Pasadena, CA, USA, in 2004.

He is currently with the Jet Propulsion Laboratory, California Institute of Technology. His research interests include the forward modeling of radar and radiometer measurements as well as retrieval of the geophysical quantity from those measurements.

Simon H. Yueh (Fellow, IEEE) received the Ph.D. degree in electrical engineering from the Massachusetts Institute of Technology, Cambridge, MA, USA, in January 1991.

He is currently a Senior Research Scientist and an SMAP Project Scientist with the Jet Propulsion Laboratory, California Institute of Technology, Pasadena, CA, USA.

Dr. Yueh is the Editor-in-Chief of the IEEE TRANSACTIONS ON GEOSCIENCE AND REMOTE SENSING.

Dara Entekhabi (Fellow, IEEE) received the B.S. and dual M.S. degrees in geography from Clark University, Worcester, MA, USA, in 1983, 1985, and 1988, respectively, and the Ph.D. degree in civil and environmental engineering from the Massachusetts Institute of Technology (MIT), Cambridge, MA, USA, in 1990.

He is currently a Professor with the Department of Civil and Environmental Engineering and the Department of Earth, Atmospheric and Planetary Sciences, MIT. He is also the Science Team Lead for the National Aeronautics and Space Administration's Soil Moisture Active and Passive mission that was launched in January 31, 2015. His research interests include terrestrial remote sensing, data assimilation, and coupled land–atmosphere systems modeling.

Dr. Entekhabi is a fellow of the American Meteorological Society and the American Geophysical Union. He is also a member of the National Academy of Engineering.